Progress Towards Acoustic Magnetized Target Fusion:
An Overview of the R&D Program at General Fusion

M. Delage, A. Froese, D. Blondal, D. Richardson

General Fusion Inc., 108-3680 Bonneville Place, Burnaby, BC V3N 4T5 (www.generalfusion.com)

michael.delage@generalfusion.com, doug@generalfusion.com

Abstract

Magnetized Target Fusion (MTF) is a hybrid approach to fusion in which a self-organized plasma is compressed with the inertia of a conductive liner to conditions that fulfill the Lawson criterion [1]. This paper provides an overview of the science behind MTF and the ongoing research at General Fusion to design, test, and demonstrate the ability to produce energy using its acoustic MTF technology.

1.   Introduction

Magnetized Target Fusion was first proposed in the 1970's as a low-cost approach to fusion that combines the advantages of magnetic confinement fusion and inertial confinement fusion by working in an intermediate regime of plasma density and confinement time. The U.S. Naval Research Laboratory did pioneering work on the LINUS program [2], which was unique among MTF schemes by employing a liquid metal liner to address the traditional fusion challenges of heat extraction, tritium breeding, and neutron flux on structural components [3,4]. The liquid liner made the compression inherently repeatable, but at the time could not be accelerated to sufficiently high velocities to compress plasma within its thermal lifetime. General Fusion is pursuing an acoustically-driven MTF concept that makes use of modern servo controllers which precisely time piston impacts to create an acoustic wave in the liquid metal liner. This wave will compress the target plasma in less than 200 µs, similar to the practically achievable plasma lifetimes in modern self-organized plasma devices. An MTF reactor with the potential to achieve net gain can be developed given current technologies.

In General Fusion's design, the deuterium-tritium fuel is supplied as a pair of magnetized plasma rings, known as compact toroids (CT). The CTs are delivered to an evacuated vortex inside a volume of liquid lead-lithium eutectic metal (atomic ratio 83% Pb, 17% Li, hereafter referred to as Pb-17Li) for the duration of an acoustically-driven spherical collapse. The cavity volume is reduced by three orders of magnitude, raising the plasma density from 10^{17} ions/cm^3 to 10^{20} ions/cm^3, the temperature from 0.1 keV to 10 keV, and the magnetic field strength from 2 T to 200 T. The fusion energy will be generated during the 10 µs that the plasma spends at maximum compression, after which the compressed plasma bubble causes the liquid metal wall to rebound. Most energy is liberated as neutron radiation that directly heats the liquid metal. Using existing industrial liquid metal pumping technology the heated liquid metal is pumped out into a heat exchange system, thermally driving a turbine generator. The cooled liquid metal is pumped back into the vessel tangentially to reform the evacuated cylindrical vortex along the vertical axis of the sphere. Liquid Pb-17Li is ideal as a liner because it has a low melting point, low vapor pressure, breeds tritium, has a high mass for a long inertial dwell time, and

has a good acoustic impedance match to steel, which is important for efficiently generating the acoustic pulse. The 100 MJ acoustic pulse is generated mechanically by hundreds of pneumatically-driven pistons striking the outer surface of the reactor sphere. The acoustic pulse propagates radially inwards, strengthened by geometric focusing from 1 GPa to 10 GPa at the surface of the vortex.

Acceleration of compact toroids (CTs) is a synthesis of two well-developed concepts: the spheromak plasma configuration and the railgun accelerator. A compact toroid is a self-organized spheromak plasma containing embedded toroidal and poloidal magnetic fields, which decays principally by resistive dissipation of the plasma currents over several hundred microseconds. A railgun switches stored electrical energy from a capacitor bank into two rails with a moving projectile acting as an armature providing a conduction path between the rails. This creates a variable-inductance line with expanding stored magnetic flux pushing the projectile and accelerating it. A CT accelerator differs from a railgun by replacing the armature-projectile with a compact toroid, which can then be accelerated to speeds in excess of 100 km/s. The CT accelerators in General Fusion's design are located at the poles of the evacuated vortex. The injected CTs travel to the center of the sphere and merge to form a stationary compressible plasma target. The plasma ions are Ohmically heated during merging by magnetic reconnection.
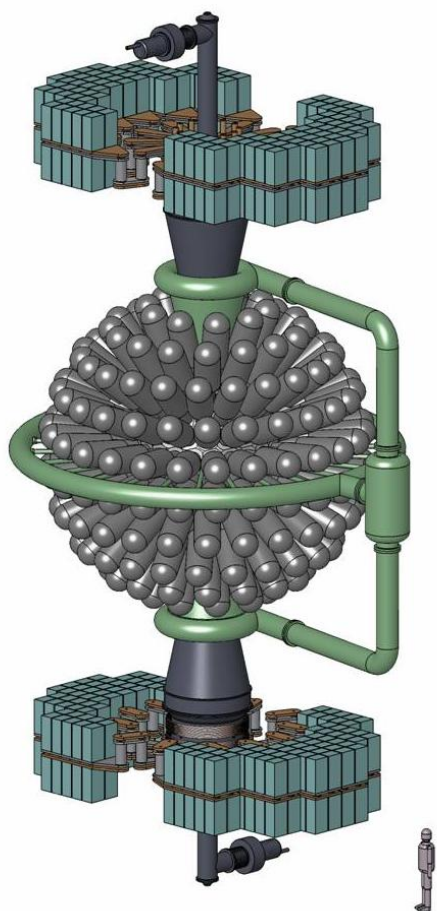
For a future power plant, economics, neutronics, tritium supply, and reactor energy density need to be considered. The eutectic absorbs the bulk of the fusion products through elastic scattering and provides a straightforward means of extracting the energy. The thick blanket significantly shields the wall by reducing the neutron flux on the structure and by lowering the neutron energy spectrum [5]. The 4 pi coverage provides an enhanced tritium breeding ratio (TBR) of 1.6 to 1.8 [6]. The neutron multiplication factor results from the Pb(n,2n) reaction and also from the ^{7}Li + n → ^{4}He + ^{3}H + n reaction as diagrammed by Moyer [7]. The challenge with a thick Pb-17Li liner is likely to be too much tritium production.

This paper summarizes General Fusion's activities during 2011 to prove the viability of its MTF technology. Efforts are focused on mitigating risks and testing full scale components for acoustically-driven compression of plasma in the proposed reactor, in order to validate the predicted plasma behaviour and demonstrate net gain. The MTF program is divided into the following areas: Acoustics Driver, Plasma Injector, and in support of these, Numerical Simulation.

Figure 1: General Fusion's Acoustic Magnetized Target Fusion Reactor Concept

2. Progress on Acoustic Driver

The servo system is now constraining piston impact timing within a 2 µs range at velocities of 40 m/s. Servo results improve with increasing speed, exceeding General Fusion's long term goals of ± 10 µs at 50 m/s. Advances in servo performance can be attributed to improvements in filtering algorithms, encoder performance, and better brake calibration and control.

Piston Servo System Repeatability Achievements						
Impact Speed	6.6 m/s	15 m/s	20 m/s	30 m/s	40 m/s	50 m/s
Timing	± 6 µs	± 16 µs	± 10 µs	± 6 µs	± 2 µs	N/A
Number of shots	>100	28	14	57	4	2

Stress testing is demonstrating materials that are capable of surviving repeated shots at velocities of 50 m/s. Modest improvements in material survivability have been made by removing stress rising features and heat-treating materials. General Fusion has been using a 1/3 scale piston system for preliminary materials testing, where heat treatment and quenching on 1/3 scale components is more effective than full scale pistons. On full-scale pistons, the most promising materials are those that are less sensitive to quench rates. Although the 50 m/s impact velocity objective has been achieved, work continues to identify tougher piston materials.

Construction of a 14-piston liquid Pb Mini-Sphere for testing vortex generation and piston impact has been completed. All piston housings have been installed once to check that they match specifications (Figure 2 top) and then removed to begin testing the Pb pumping system (Figure 2 left). The pumping system contains 15 tonnes of Pb storage and can sustain a 100 kg/s mass flow rate. In addition to the vessels, piping, and electrical systems of the Pb handling system, Figure 2 also shows trenches and pits that have been added to the concrete slab floor to safely direct Pb flow in case of accidental leakage.

2.1 Vortex Diagnostics

Liquid Pb vortices have been created in the Mini-Sphere and pressure pulse testing is anticipated to commence shortly. Several diagnostic techniques have been investigated as part of an ongoing effort to prepare for interpreting data from the Mini-Sphere and for later use in higher energy experiments.

Optical: Positive results have been obtained with diffuse light sources mounted in line with a camera pointing into the Mini-Sphere from above. The setup is shown in Figure 3a and one of the first images captured of the vortex is shown in Figure 3b. In addition, a photoelectric distance sensor that is capable of scanning the shape of the free surface of the Pb is currently being installed.

Ultrasonic imaging: The position of the central vortex in a water-filled sphere has been successfully determined by measuring the time-of-flight of a sound pulse from a single source to two remotely located receivers. However, the extreme conditions in the Mini-sphere will present unique challenges for the ultrasound sensors that General Fusion is working to mitigate. These include wetting the sensors in liquid metal, high temperatures, strong pressure waves, and the frequency response of the sensors.
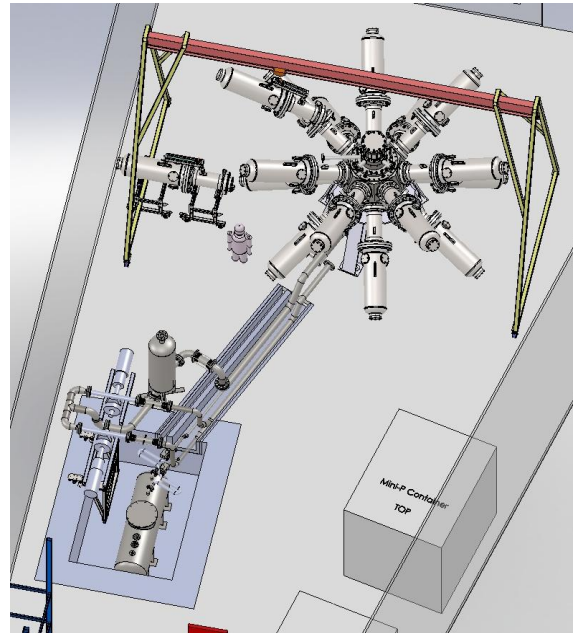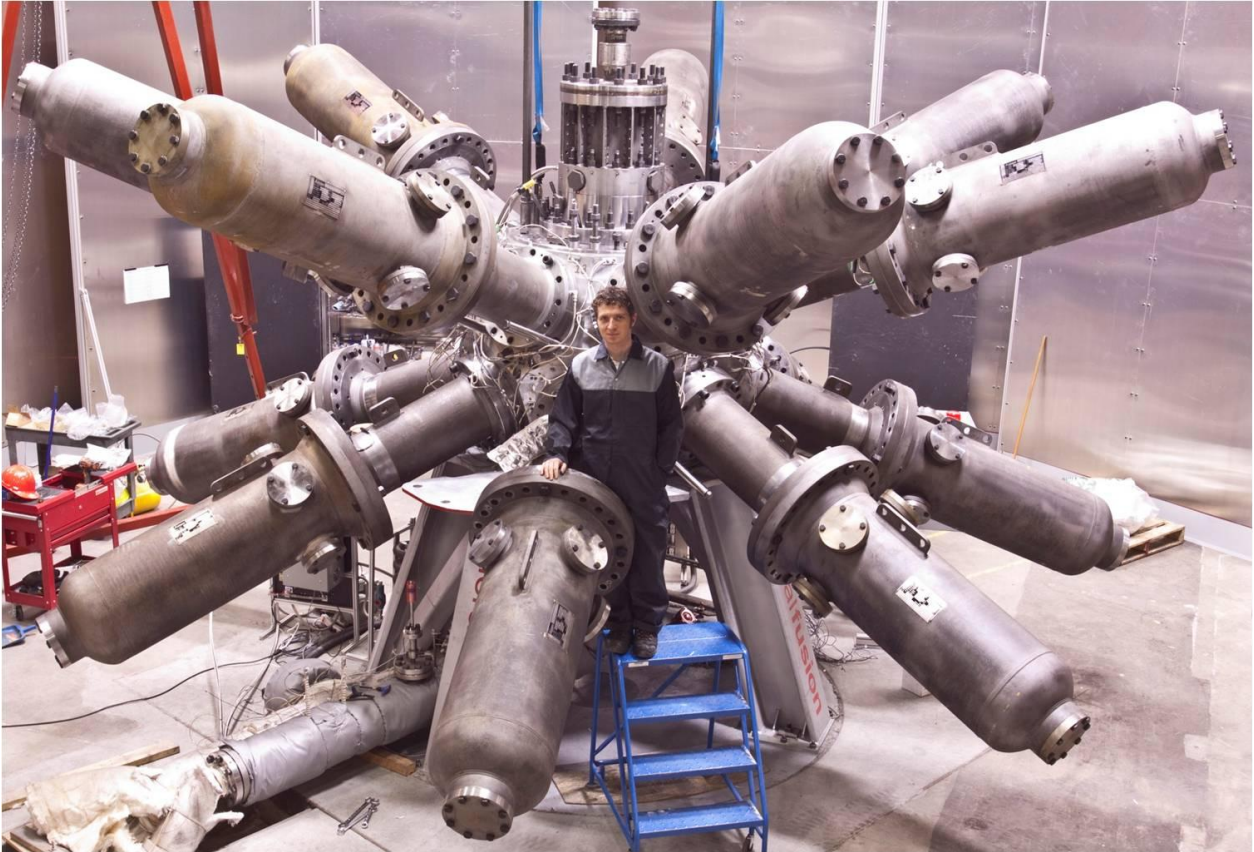
Figure 2: (Top) Photograph of the Mini-Sphere with piston housings installed. (Left) Photograph of the Pb pumping system including Pb pumps, melt vessel, de-bubbling vessels, and a section of Pb piping. (Right) Schematic of the 14-piston liquid Pb Mini-Sphere connected to the Pb pumping system.
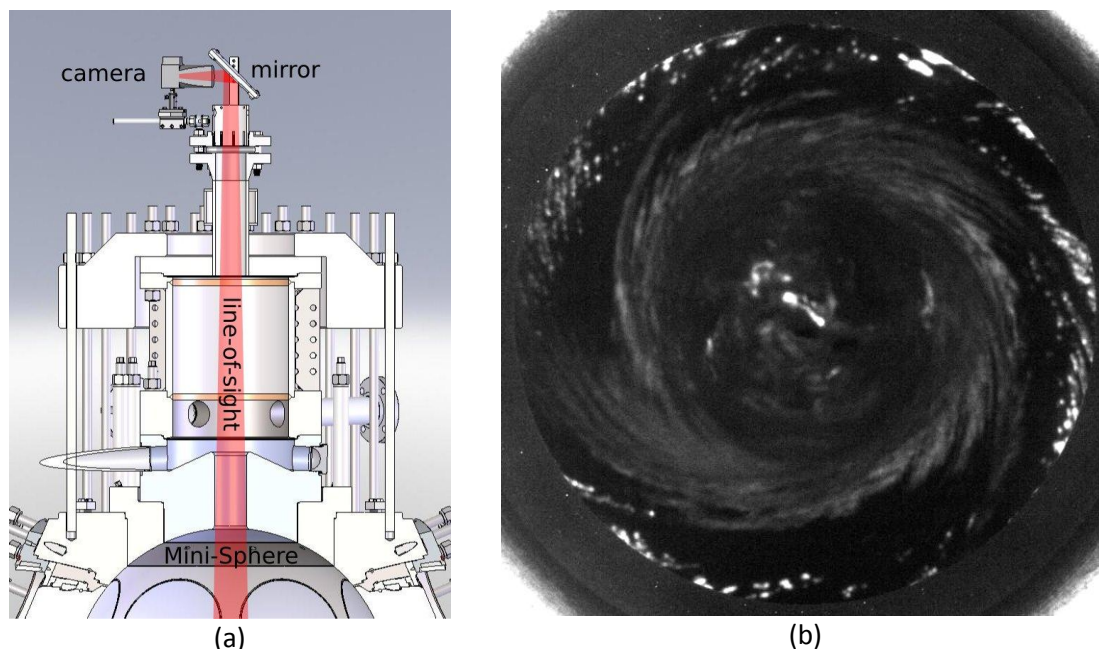
(a)   (b)

Figure 3: (a) Schematic showing line-of-sight from the optical camera to the Pb vortex. (b) Early image of liquid Pb draining from the Mini-Sphere.

Pressure Sensors: Pressure sensors must be capable of measuring pressures up to 1 GPa with microsecond resolution while operating in a conductive medium at temperatures in excess of 400 Celsius. Fiber Bragg Gratings (FBGs) are the most promising as they are used to study explosive wave fronts. Another possible method is the use of strain gauged collapsible tubes, which were tested on the Mini-Piston when it was filled with PbBi.

2.2   Cavity collapse simulations

Extensive computational fluid dynamics (CFD) and finite element analysis (FEA) numerical testing has been performed to design the Mini-Sphere (Figure 4a). Models were made to predict pressure wave propagation and the shape of vortex collapse by testing different piston impact velocities, impact timings, piston positions, and reactor shapes. Due to the small size of the Mini-Sphere, the 14 pistons are expected to compress the vortex from the center towards the poles. Simulations have shown that compression from the poles to the center on a larger system can be accomplished by timing the piston impacts to create an oblate spheroidal wave front.

Identifying and reducing potential damage to the Mini-sphere and its auxiliary systems is an important role of modeling. For example, estimations of "Water hammer" behaviour in the Mini-Sphere have indicated that the pressure wave initiated by the pistons will enter the pumping system (Figure 4b). Methods for mitigating damage to the pipes and Pb pumps are being investigated and simulated to calculate the forces on the supporting structure resulting from asymmetric firing of the 14 pistons.

Figure 5 shows initial predictions of the hydrodynamic Richtmyer-Meshkov instability that develops during vortex collapse, affecting the compression and heating of the plasma. Results will help identify the degree to which the vortex surface must be kept smooth.

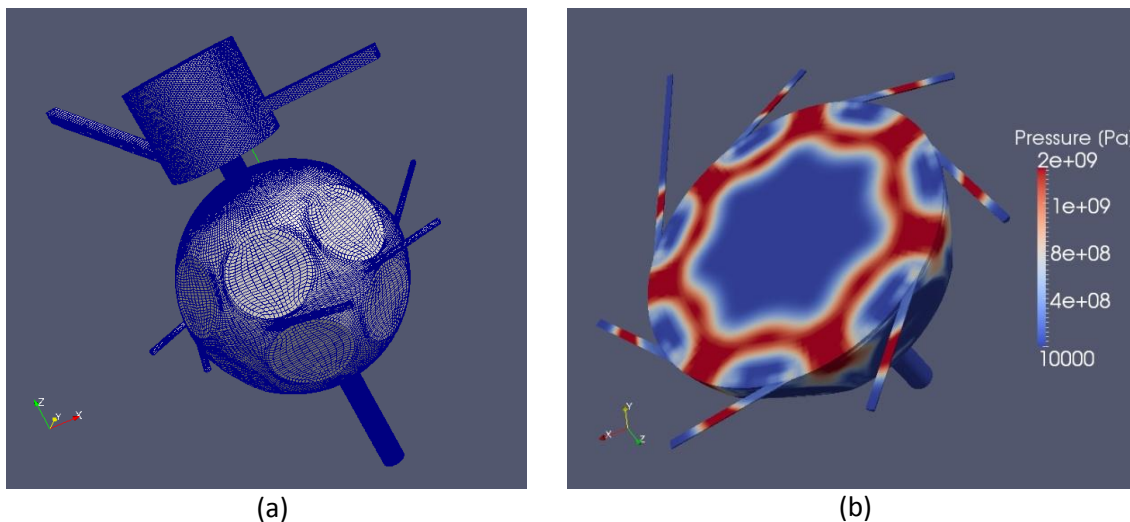(a)   (b)

Figure 4: (a) Computational grid for compressible simulation of Mini-Sphere. (b) Pressure field developed inside the sphere and pumping pipes shortly after pistons striking the Pb. Pressure pulse ("water hammer") occurring in the pumping system is seen by red areas in the pumping pipes.
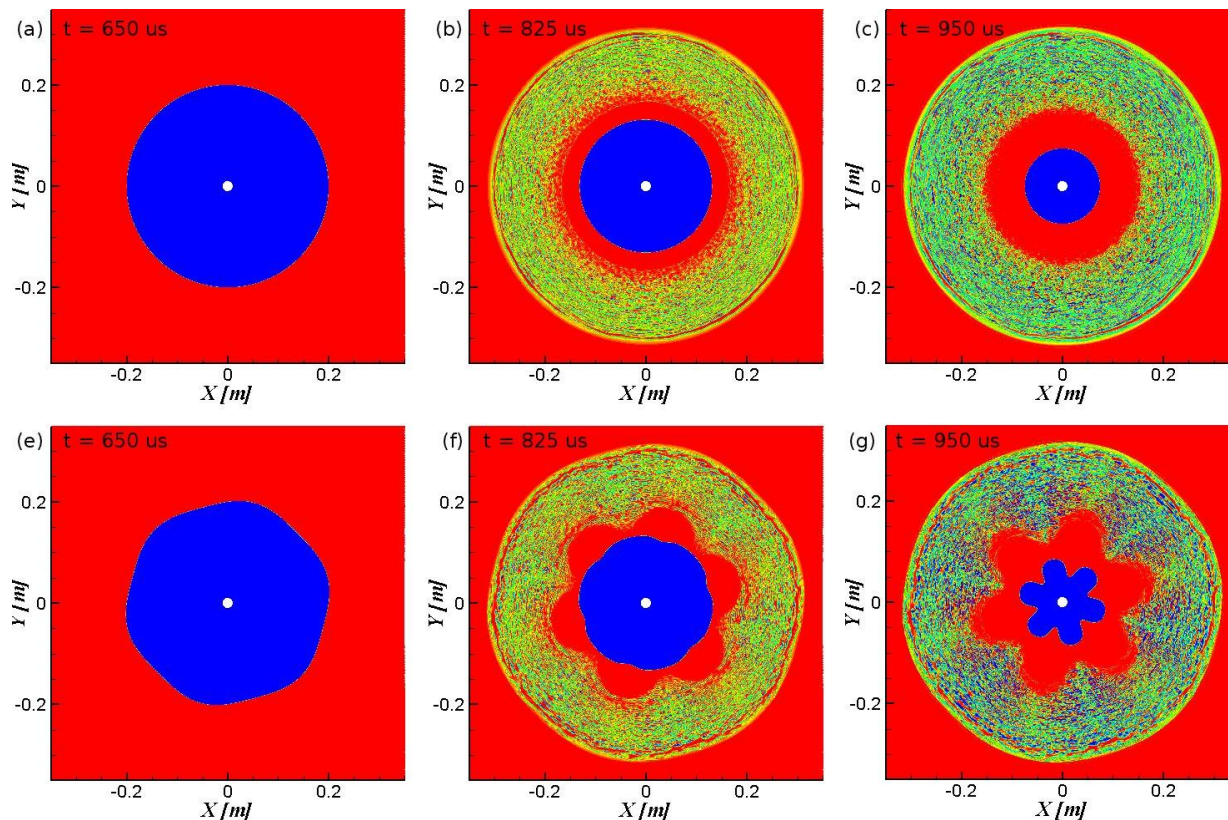

Figure 5: Compressible multiphase simulations done with OpenFoam showing the development of the Richtmyer-Meshkov instability during the cylindrical collapse of an air-filled vortex. (a) Initial vortex interface without perturbation. (b,c) Cavitation region (speckled) appears as pressure pulse pushes interface inward. (d) Vortex interface with an initial 2.5% perturbation. (e) Smoothing of the disturbance (phase inversion) during the the early stages of collapse. (f) Distortion of the interface at later stages of collapse due to R-M instability. Rotation of the Pb and magnetic pressure, which have a stabilizing effect, are not taken into account at this stage.

3.   Progress on Plasma Injector

The various steps involved in creating and compressing a CT in the plasma injector are shown in Figure 6.   The plots show the poloidal current as calculated in an axisymmetric magnetohydrodynamic simulation done with VAC, (Versatile Advection Code).   (a) Initially, a voltage is applied to the formation electrode, which increases the toroidal magnetic field in the formation region.   (b) The toroidal field interacts with the poloidal stuffing field to bubble out a CT. (c) The CT separates from the stuffing field and sits in the formation region. (d) A voltage is then applied to the acceleration electrode, increasing the toroidal field behind the CT and pushing the CT down the injector. (e) Sometimes the thermal pressure in the CT becomes larger than the pushing force applied by the acceleration current, causing it to slow down. (f) The energy capacitors and injector are analogous to an LRC circuit, so the accelerator voltage oscillates after pushing the CT to the target chamber.

General Fusion has made progress in forming and accelerating compact toroids (CT) and is nearing the requirements for long lasting, stable, and hot CTs in the target chamber. The typical plasma parameters listed in the following table demonstrate a compression factor of approximately 16.

Metric	Plasma Formation Achievements to date
Magnetic field lifetime	70 µs in the target chamber
Magnetic field strength	0.12 Tesla in formation, 2 Tesla near the target chamber
Plasma Density	1-2 x 10^{16} cm^{-3} line averaged, 6 x 10^{16} cm^{-3} peak
Mass	0.9 mg @ 1×10^{16} cm^{-3}
Temperature	50-100 eV (electron), 100-200 eV (ion)
Reliability	9 out of 10

Early testing of the plasma injector was characterized by poor efficiency due to stray plasma within the bus work of the inner vacuum vessel, allowing the acceleration current to short across to the interior grounded pumping chamber. In addition, break down pathways during acceleration caused excessive arcing to the outer vacuum vessel. A typical example of these arcs is shown in Figure 7a.

A series of design changes were implemented and tested, eventually resulting in the elimination of the asymmetric acceleration fields and arcing (Figure 7b). With alternative pathways removed, the acceleration current now delivers most of its energy to the CT, allowing it to reach elevated temperatures and magnetic fields.

Performance increases were also achieved by improving the axisymmetry of the gas density prior to discharge. Gas is injected into the vacuum vessel through 50 puff valves near the back of the formation region. It was found that the volume of gas being injected was not equal; a small number of valves were injecting far more gas than average each shot. Synchronizing the timing and equalizing the injection volume of all the puff valves reduced fluctuations in the formation plasma density, as shown in Figure 7c.
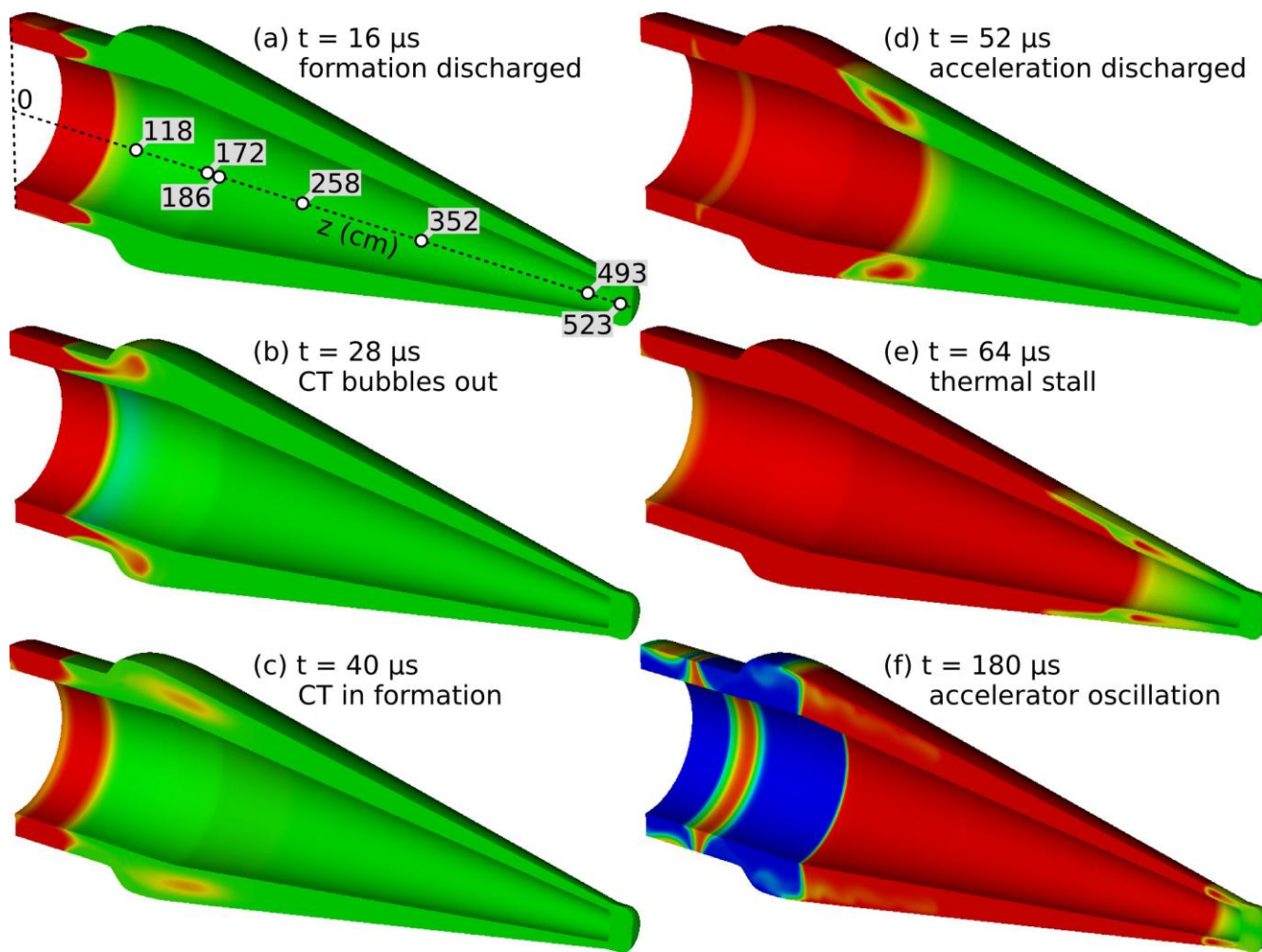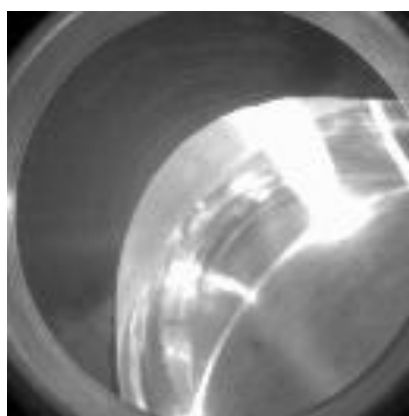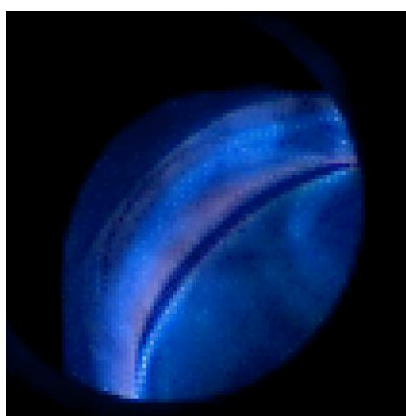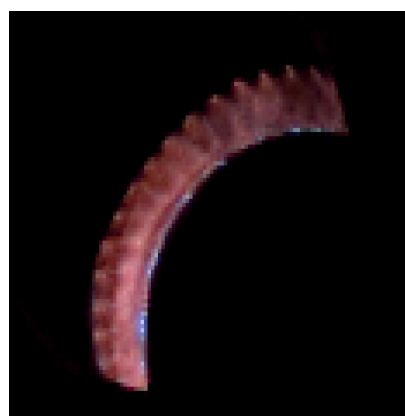
Figure 6: Simulation of poloidal current in the plasma injector done with VAC (red positive, blue negative). Axial positions of probe ports are marked by white circles in (a).

(a) Arcing between inner and outer electrodes.

(b) Arcing is gone between inner and outer electrodes.

(c) Puff valve symmetry in formation area.

Figure 7: Still frames from high speed videos showing plasma in the formation and acceleration regions.

3.1 Electron and Ion Temperatures

The Thomson scattering system is the primary temperature diagnostic for the plasma injector. It has been recently upgraded to a 16 channel photomultiplier tube array to increase sensitivity. Measurements are now possible at much lower densities than in the past, giving access to temperature data in the formation region. Figure 8a charts an ensemble of Thomson scattering temperature snapshots at various times after the CT is formed (without acceleration.) The time scales are consistent with resistive decay of the magnetic fields. Figure 8b shows a similar ensemble measured near the target chamber with a typical magnetic field and density for the same location are shown superimposed. These results indicate that the electron temperatures are elevated (60-80 eV) on the leading edge of the CT and cooler (20-40 eV) at the density peak and on the trailing edge, although it is presently difficult for Thomson to make clear temperature measurements using Thomson scattering at the time of the peak density because the plasma light can saturate the detectors.

Ion Doppler temperature measurements have been added to complement the Thomson electron temperature measurements. They are based on Doppler broadening of spectral lines from helium and oxygen in the plasma. Ion Doppler results are more difficult to interpret than Thomson scattering results, but can be performed at more than one location and more than one time each shot, potentially providing much more information that Thomson scattering. Ion Dopper results taken during a single shot at 5 different points are shown in Figure 8c. They clearly show temperature rising from 50 eV near the beginning of the acceleration region (position 172) to 100-150 eV in the target chamber (position 523). More recent results suggest ion temperatures as high as 200 eV prior to entering the target chamber. Studies with other CT devices have shown that ion temperatures are consistently greater than electron temperatures [8,9].

3.2 Plasma Lifetime

The density of the plasma in the target chamber (position 523) has been measured to be greater or equal to that measured just outside it (position 493). Both density and temperature are thus quite close to those required for compression experiments. The third element required for successful compression is to have relatively stable plasma in the target chamber with a lifetime greater than 100 μs. General Fusion is currently achieving lifetimes in the chamber of 50-80 μs, but this can be extended considerably by optimizing the timing of the accelerator current. Ideally the accelerator current should begin to drop soon after the back edge of the CT reaches the target chamber, but instead continues to apply pressure that disturbs the magnetic structure of the CT.

Excess acceleration current will not present a problem in future merging experiments. Work has begun on a second plasma injector, which will be connected to the first injector. An evacuated drift tube will run between the injectors taking the place of the Pb vortex. When the injectors are fired simultaneously, a pair of high-speed CTs will meet in the drift tube and combine to become a single CT with a stronger magnetic field and longer lifetime. In addition, replacing the target chamber with a drift tube will allow the excess acceleration current to be converted into the kinetic energy of the CT.

(a)

Position z = 118 cm is at the widest point of the injector, where the CT is first formed

(b)

(c)

Position descriptions

172 and 186 cm: CT formation area, no radial compression

352 cm: halfway along the injector, approx. 2X radial compression, 8X volume compression

523 cm: in flux conserver at end of injector, approx. 4X radial compression, 64X volume compression
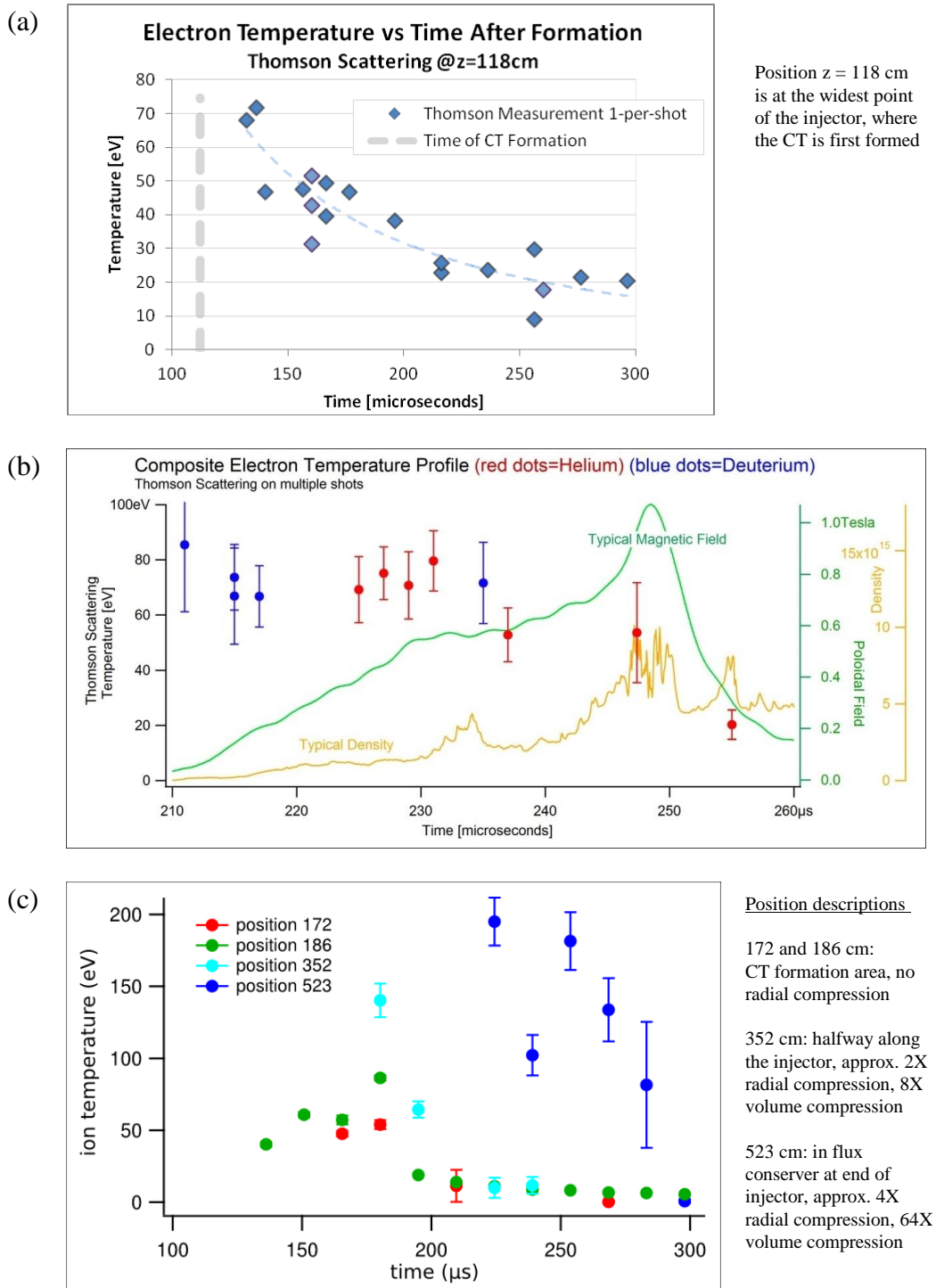
Figure 8: (a) Composite time history shows that the CT is formed at temperatures well above 50 eV and then cools on time scales consistent with resistive decay of the magnetic fields. (b) Temperature for both deuterium (blue) and helium (red) plasmas, shown with typical magnetic field (green) and density (orange) time profiles near the target chamber. (c) Ion Doppler broadening temperature measurements over time for 5 different locations in the injector.
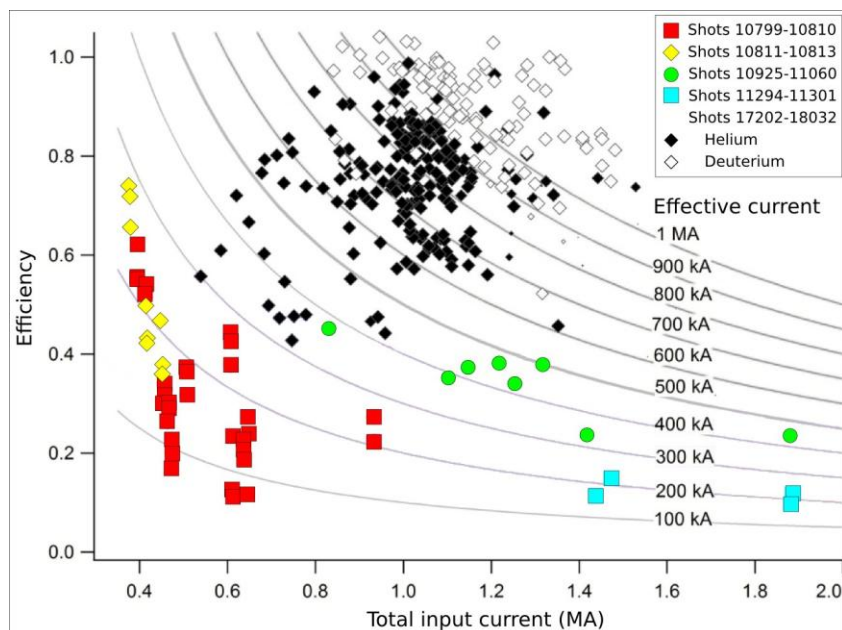
Figure 9: Acceleration efficiency versus input current for various injector configurations. Shots from March and April 2011 are indicated by coloured points. Shots from October 2011 are indicated by white diamonds for deuterium and black diamonds for helium.

3.3   Accelerator Efficiencies

The acceleration efficiency is defined as the ratio of current that passes position 118 as measured by the magnetic probes and the input current as measured by the Rogowski coils on the input bus rods. The acceleration efficiency of the plasma injector is limited by plasma activity within the bus work of the inner vacuum vessel and in the vicinity of the acceleration gap. Acceleration current that is diverted through this stray plasma reduces the amount of current available to push on the CT. Therefore, this quantity is a useful metric for evaluating changes to the injector configuration.

The acceleration efficiency for various injector campaigns, each with a different configuration, is shown in Figure 9. Past campaigns had failed to put more than 500 kA into acceleration, regardless of input current (coloured points). Shots from the October 2011 campaign appear as black and white diamonds and indicate a clear improvement, with acceleration efficiencies approaching unity. This supports the theory that arcing was reducing the energy available for accelerating the CT. Arcing in the outer vacuum vessel is eliminated for 100% of the shots and eliminated in the inner vacuum vessel for more than 90% of these shots.

Figure 9 suggests that deuterium shots have systematically better acceleration efficiencies than helium shots. While this may be partially true, the deuterium shots were run more recently and benefit from continued learning and improving vacuum conditions. Nonetheless, more than 90% of deuterium shots exhibit better than 70% pushing efficiency.

4.   Summary

The previous year has seen much progress towards creating and compressing plasma and the outlook is now very encouraging. In particular, plasma densities of 10^{16} ions/cm^3 at 50-100 eV electron temperatures and up to 200 eV plasma ion temperatures have been demonstrated with 90% repeatability and the magnetic lifetime in the target chamber is between 50 and 80 µs. Piston impact speeds of 50 m/s and servo-controlled impact timing accurate to ±2 µs have been achieved. The 14-piston liquid Pb Mini-Sphere assembly for testing vortex generation and piston impact has been completed and is ready for experimentation to begin.

General Fusion is buoyed by recent progress on all fronts of the MTF program. Improvements in piston survival, liquid Pb handling, plasma temperature, acceleration efficiency, injector reliability, and regulatory matters have left the team and investors with a positive outlook on the coming year and the company's ability to meet goals.

5.   Acknowledgements

6.   References

[1]   J. D. Lawson, "Some Criteria for a Power Producing Thermonuclear Reactor", *Proceedings of the Physical Society. Section B*, Vol. 70, Iss. 1, 1957.

[2]   R. L. Miller and R. A. Krakowski, "Assessment of the slowly-imploding liner (LINUS) fusion reactor concept", 4th ANS Topical Meeting on the Technology of Controlled Nuclear Fusion, 1980 October 14-17.

[3]   R. Siemon, I Lindemuth, K. Schoenberg, "Why Magnetized Target Fusion Offers A Low-Cost Development Path for Fusion Energy", Comments on Plasma Physics and Controlled Fusion, 1997.

[4]   R. Siemon *et al.,* "The relevance of Magnetized Target Fusion (MTF) to practical energy production, a white paper for the Fusion Energy Sciences Advisory Committee", *Los Alamos National Labs,* 1999,
http://fusionenergy.lanl.gov/Documents/MTF/MTF_Appl._whitepaper_6-99.PDF

[5]   D. Dudzick, "Nucleonic aspects of the LINUS imploding blanket", ANS Meeting on the Technology of Controlled Thermonuclear Fusion, Santa Fe, New Mexico, USA, 1978 May 9.

[6]　　M. E. Sawan, M. A. Abdou, "Physics and technology conditions for attaining tritium self-sufficiency for the DT fuel cycle", *Fusion Engineering and Design*, Vol. 81, 2006, pp. 1131-1144.

[7]　　M. Moyer, "Fusion's False Dawn", *Scientific American*, March, 2010**,** pp. 50-57.

[8]　　P.M. Bellan, *Spheromaks* (Imperial College Press, Copyright 2000), pp 222.

[9]　　R.M. Mayo, et al., *Nucl. Fusion* **31** (1991) pp 2087.